JACS
JOURNAL OF THE AMERICAN CHEMICAL SOCIETY

Communication

pubs.acs.org/JACS

Hydrogen-Bond Symmetrization Breakdown and Dehydrogenation Mechanism of FeO_2H at High Pressure

Sheng-cai Zhu,[†] Qingyang Hu,[*,†,‡] Wendy L. Mao,[‡] Ho-kwang Mao,[†,§] and Hongwei Sheng[†,∥]

[†]Center for High Pressure Science and Technology Advanced Research (HPSTAR), Shanghai 201203, People's Republic of China
[‡]Department of Geological Sciences, Stanford University, Stanford, California 94305, United States
[§]Geophysical Laboratory, Carnegie Institution of Washington, Washington, D.C. 20015, United States
[∥]Department of Physics and Astronomy, George Mason University, Fairfax, Virginia 22030, United States

HPSTAR 431-2017

Supporting Information

ABSTRACT: The cycling of hydrogen plays an important role in the geochemical evolution of our planet. Under high-pressure conditions, asymmetric hydroxyl bonds tend to form a symmetric O−H−O configuration in which H is positioned at the center of two O atoms. The symmetrization of O−H bonds improves their thermal stability and as such, water-bearing minerals can be present deeper in the Earth's lower mantle. However, how exactly H is recycled from the deep mantle remains unclear. Here, we employ first-principles free-energy landscape sampling methods together with high pressure-high temperature experiments to reveal the dehydrogenation mechanism of a water-bearing mineral, FeO_2H, at deep mantle conditions. Experimentally, we show that ∼50% H is released from symmetrically hydrogen-bonded ε-FeO_2H upon transforming to a pyrite-type phase (Py-phase). By resolving the lowest-energy transition pathway from ε-FeO_2H to the Py-phase, we demonstrate that half of the O−H bonds in the mineral rupture during the structural transition, leading toward the breakdown of symmetrized hydrogen bonds and eventual dehydrogenation. Our study sheds new light on the stability of symmetric hydrogen bonds during structural transitions and provides a dehydrogenation mechanism for hydrous minerals existing in the deep mantle.

The transportation and circulation of water from Earth's surface to its deep interiors plays a key role in the chemical properties of mantle minerals.[1−3] Common layered hydrous minerals often have low densities and relatively low thermal stability. Consequently, they dehydrate before reaching the bottom of Earth's transition zone.[4,5] However, recent high pressure−temperature ($P-T$) experiments suggest that a family of dense hydrous silicates and hydroxides could carry water to deeper zones (>1800 km depth) of the lower mantle because of the formation of strong symmetric hydrogen bonds (SHB).[6−8] The rigid SHB due to the shortening of the O···O distances compresses the lattices and is the favorable configuration for many high-pressure phases of hydroxyls, such as ice X,[9,10] δ-AlO_2H,[11] the H-silicate phase,[7] ε-FeO_2H[12] and the pyrite-type FeO_2Hx[13] ($0 < x < 1$). For the same chemical composition, these SHB-based polymorphs have higher thermal stability owing to greater O−H−O binding energies than their asymmetric counterparts.[11,14] However, FeO_2H was observed to release H_2 upon the phase transition to the Py-phase at conditions found in the deep lower mantle.[13] The dehydrogenation behavior of FeO_2H suggests that the SHB network weakens as it transforms to the Py-phase and that the symmetric hydrogen bonds must break in order to release H. Many questions remain unresolved concerning the phase transition and the dehydrogenation mechanism. Here, we aim to unravel the atomistic mechanism underlying the dehydrogenation process of ε-FeO_2H and understand the behavior of the SHB upon the phase transition from ε-FeO_2H to the more stable Py-phase.

To model this phase transition, we employ a recently developed stochastic surface walking (SSW) method integrating density functional theory (DFT) for crystal sampling.[15,16] One advantage of this method is that it is capable of exploring new structures and reaction pathways by sampling the energy landscape exhaustively and unbiasedly. Followed by the double-ended surface walking approach,[17] the transition state (TS) can be located among the pathways harvested by the SSW sampling method. On the basis of the sampled free energy landscape, the pathways connecting the initial structure and the final structure on the potential energy surface can be determined in an atom-to-atom correspondence which can be seamlessly exported to further structural analysis such as the nudged elastic band (NEB) method.[18] The SSW method has been used successfully to predict the low-energy pathways of crystal phase transitions (e.g., TiO_2,[19] ZrO_2[20] and MnO_2[21]), surface reconstruction[22] and molecular reactions.[23]

This study explores the structural transformation between two high-pressure FeO_2H phases, ε-FeO_2H and Py-FeO_2Hx. The Fe and O atoms in the ε-FeO_2H lattice form a $CaCl_2$-type structure which is the thermodynamically stable structure above a few gigapascals (GPa).[24] The Py-phase, on the other hand, is experimentally found to be stable at higher pressures (>72 GPa).[13] This $CaCl_2$-type to pyrite-type structural transition has recently drawn great attention due to an unexpected large-volume collapse associated with the partial release of H.

The SSW-crystal method was performed using the plane wave density functional theory program, Vienna *ab initio*

Received: June 23, 2017
Published: August 22, 2017

DOI: 10.1021/jacs.7b06528
J. Am. Chem. Soc. 2017, 139, 12129−12132

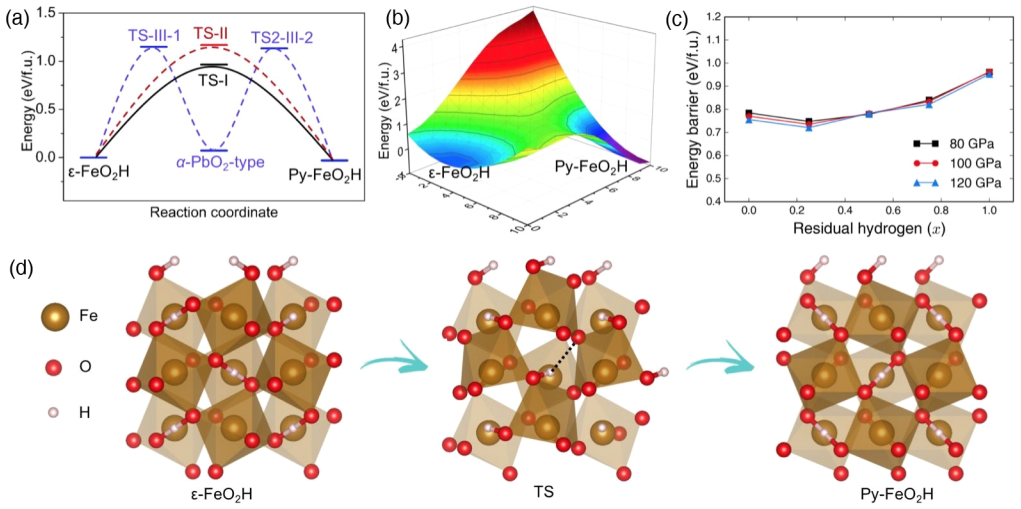

Figure 1. (a) Potential energy profiles connecting ε-FeO_2H and Py-FeO_2H by the SSW method. (b) Potential energy surface of transition path I obtained by linear interpolation of lattice parameters and atomic fractional coordinates from structure snapshots. (c) Energy barrier at 80, 100 and 120 GPa with different hydrogenation level x. (d) Structural evolution following path I viewed from the normal direction of the atomic habit plane $(110)_\varepsilon$ or $(100)_{Py}$. The dashed line in the TS indicates the breakdown of a symmetrized hydrogen bond.

simulation package[25] where the electron−ion interactions of Fe, O and H atoms are represented by the projector augmented wave[26] scheme. The exchange-correlation functional is described by the generalized gradient approximation in the Perdew−Burke−Ernzerhof parametrization.[27] The pathway sampling was carried out in a 16-atom (4 FeO_2H units per cell) lattice for both the ε and Py-phases. Through our exhaustive SSW sampling, a large set (in the order of 10^3) of initial/final state pairs was collected at 80 GPa. We located the TS by the double-ended surface walking approach and refined candidate pathways by sorting the heights of computed energy barriers. Furthermore, we performed a strain analysis following the finite strain theory and obtained the strain-invariant plane, identified as the habit plane. The stability of the interfaces was evaluated by considering the interfacial energy,[28] defined as $\gamma = (E_{tot} - E_a - E_b)/2S$, where S is the interfacial area, E_a and E_b are the energies of the parent phases, and E_{tot} is the energy of the mixed phase. The most favored pathway was determined from both the energy barrier and the interfacial energy.

Among the shortlist of 50 pairs of ε-FeO_2H/Py-FeO_2H paths from hundreds of possibilities, three lowest energy pathways from ε-FeO_2H (*Pnnm*, no. 58) to Py-FeO_2H ($Pa\bar{3}$, no. 205) were identified, namely paths I, II and III. The overall potential energy profiles of these pathways are shown in Figure 1a,b. The calculated lowest energy barrier of path I is 0.96 eV/formula unit (f.u.) relative to the ε-phase. Path I is a direct pathway with the orientation relation of $(110)_\varepsilon//(001)_{Py}$, $[001]_\varepsilon//[100]_{Py}$. The computed $(110)_\varepsilon//(001)_{Py}$ interfacial energy of path I is found to be the lowest, ~0.362 J/m^2. These interfaces are determined to be the minimum strain planes, evidenced by the closely matched lattice parameters, e.g., $(110)_\varepsilon = 4.777 \times 4.505$ $Å^2$ and $(001)_{Py} = 4.453 \times 4.453$ $Å^2$, as summarized in Table S1. It should be mentioned that, although Fe cations may transform from high spin to low spin during compression, spin-polarized DFT calculations yield similar energy barriers (e.g., 0.91 eV/f.u. for path I) and do not change the order of favorable pathways. Therefore, we conclude that the energy barrier separating ε-FeO_2H and Py-FeO_2H results mainly from the atomic displacements rather than from the change of spin states. The spin effect will not be discussed in the rest of this work. Compared to path I, the other two paths require overcoming much higher energy barriers (1.16 eV/f.u. for path II and 1.15 eV/f.u. for path III, respectively). The crystallographic orientation relation of path II is $(101)_\varepsilon//(001)_{Py}$, $[010]_\varepsilon//[100]_{Py}$. Unlike paths I or II, path III tunnels through an intermediate orthorhombic phase, namely the α-PbO_2-type phase (*Pbcn*, no. 60). Its overall crystallographic orientation relation is summarized as $(101)_\varepsilon//(001)_\alpha$, $[010]_\varepsilon//[100]_\alpha$, $(001)_\alpha//(001)_{Py}$ and $[100]_\alpha//[100]_{Py}$. Because of the large lattice mismatch in the interface of paths II and III (20% strain) and significantly higher interfacial energies (2.884 and 3.112 J/m^2, respectively in Table S1), path I is determined to be the most preferred pathway for the transition from ε-FeO_2H to Py-FeO_2H.

Figure 1d depicts the initial state, TS and the final state along path I. The SSW method automatically converts the orthorhombic ε-FeO_2H to its equivalent monoclinic unit cell to match the structural transition (details in SI). We find that the transition is essentially a diffusionless martensitic phase transition in nature, resulting in the reconstruction of Fe−O octahedra connected by O−H bonds. Along the path, the ε-FeO_2H lattice (a = 4.505, b = 4.777, c = 4.777 Å, α = 61.80°, $\beta = \gamma$ = 90°) transforms to the Py-FeO_2H lattice ($a = b = c$ = 4.453 Å, $\alpha = \beta = \gamma$ = 90°) with 2.6% volume collapse. Obviously, the initial and the final lattices share many similarities except for a difference in the lattice angle α ($\Delta\alpha$ = 28.20°), which is the dihedral angle between the $(110)_\varepsilon$ and $(1\bar{1}0)_\varepsilon$ planes in the ε-FeO_2H phase and the dihedral angle between the $(001)_{Py}$ and $(010)_{Py}$ planes in the Py-phase. Microscopically, the phase transition initiates via rotation and shearing of the close-packed $(101)_\varepsilon$ atomic plane of ε-FeO_2H. During the atomic rearrangements on the $(101)_\varepsilon$ plane, two Fe−O and two O−H bonds break, resulting in the formation of two 5-coordinated Fe (Fe_{5c}) and two 3-coordinated O (O_{3c}) at the TS. Following the TS, Fe_{5c} creates new bonds with O_{3c}, leading to the completion of Py-FeO_2H. The atoms shuffle along the $[1\bar{1}0]_\varepsilon$ direction (in parallel to the habit plane) and reduce the angle difference between the two lattices. As soon as the $(101)_\varepsilon$ plane in ε-FeO_2H evolves into the $(001)_{Py}$ plane in Py-FeO_2H, two more Fe−O bonds break between the first and

DOI: 10.1021/jacs.7b06528
J. Am. Chem. Soc. 2017, 139, 12129−12132

second layers, and $(110)_\varepsilon$ moves parallel to $(001)_{Py}$. During the transition, atoms displace only on the first layer (Figure 1d) and the SHBs pertaining to the second layer remain stable. Apparently, only half of the SHBs on the first FeO_2H layer break by rotation and shearing along the $[1\bar{1}0]$ direction. The transition signifies the breakdown of the SHBs at the TS.

To understand the effects of pressure and the depletion of H on the phase transition kinetics, we calculated the phase transition energy barrier of FeO_2Hx (x = 0, 0.25, 0.5, 0.75 and 1) at different pressures. The removal of H atoms follows the rule to achieve the highest possible lattice symmetry. In Figure 1c, the energy barrier is slightly lowered with reduced H content. For example, the energy barrier drops by 12.8% after removing the first H and further drops by an additional 6.6% after removing a second H on the first layer. Our results suggest that releasing H atoms promotes the transition kinetics by lowering the transition energy barrier. On the other hand, a large increase in pressure (80 GPa compared to 120 GPa) only slightly reduces the barrier height (e.g., 0.01 eV/f.u.). Hence, our theoretical calculation corroborates our experimental observation that pressure has an almost negligible effect on the kinetics of this phase transition.[17]

It is worth mentioning that in MO_2-type materials (e.g., SiO_2[29] and TiO_2[30,31]), the $CaCl_2$-type structure transits to the pyrite phase via an α-PbO_2-type structural intermediate. However, for FeO_2H, the energy barrier of the similar indirect pathway via an α-PbO_2-type phase (see Figure 1, path III) is ~0.2 eV/f.u. higher than that path I, which leads to a reaticon rate approximately 3500 times slower than that of path I based on the transition state theory.

The theoretically obtained transition pathway was verified by our high P–T X-ray diffraction (XRD) experiments, as shown in Figure 2. In the experiment, ε-FeO_2H was laser-heated at

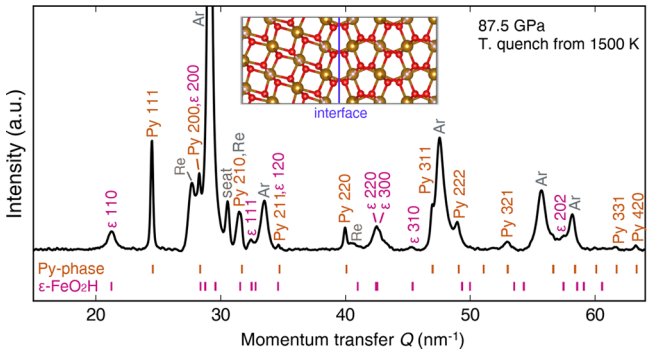

Figure 2. XRD pattern showing the coexistence of ε-FeO_2H and Py-phase in Ar at 87.5 GPa after quenching from 1500 K. Inset shows the ε-FeO_2H and Py-phase interface.

87.5 GPa and 1500 K using in a diamond anvil cell (details in SI). The peaks can readily index into a coexisting mixture of ε-FeO_2H and Py-phase. The coexistence of the two end products is due to an ongoing transition at a relatively low temperature (1500 K) and short heating duration (<1 min). No diffraction peaks associated with the α-PbO_2-type structure (or other phases) was detected throughout out these experiments.

An equally important observation in our experiment is that the formation of Py-phase FeO_2Hx is accompanied by the release of H.[2,13] We have determined the residual amount of hydrogen in the Py-phase, x, as a function of pressure based on the volume changes of FeO_2Hx, as shown in Figure 3. From a

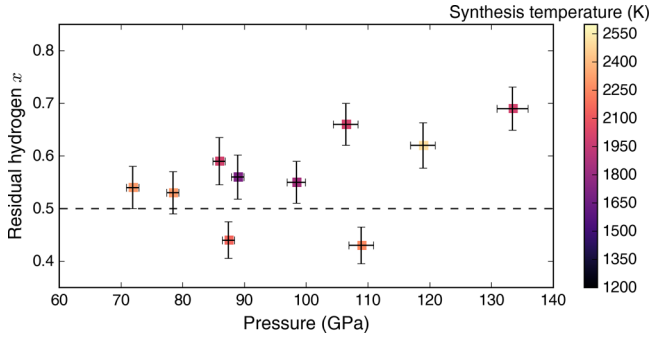

Figure 3. Pressure vs x in the Py-phase. Errors in x are estimated from volume change uncertainties of the Py-phase. Temperature variance is up to 300 K.

series of experiments on the formation of py-FeO_2Hx, the residual H content x is found to approach 0.5 within our estimation errors. The partial release of H, or $x \sim 0.5$, agrees well with the theoretical prediction in Figure 1d, in which half of the SHB network breaks during the phase transition.

So far, combining both the SSW method and the experiment, we have explored the mechanism of H release. The exact structural evolution along path I has yet to be resolved on the atomistic level. To this end, we revisited the pathway by employing the solid-state NEB (ssNEB) method[18] (details in SI). Figure 4a is the change of enthalpy in path I from 18

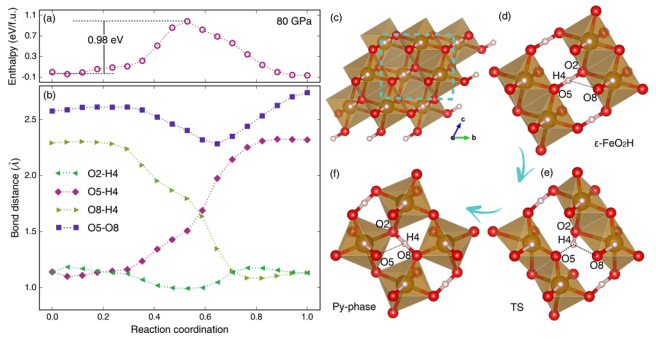

Figure 4. Transition path obtained with the ssNEB method. (a) Enthalpy barrier from ε-FeO_2H to Py-FeO_2H. (b) Changes of relevant O–H and O–O bonding distances along the transition path. (c) The highlighted area in the initial ε-FeO_2H is zoomed in for structural evolution from (d) the ε-FeO_2H to (e) TS and (f) the Py-FeO_2H.

structural replicas. The transition state at the saddle point matches the TS derived from the SSW method. On the formation layer where O–H bonds break, we collected a representative group of atoms and tracked their interatomic distances. Following the phase transition, the distance of O5–H4 increases from 1.14 to 2.32 Å, whereas O8 approaches H4 from 2.29 to 1.13 Å, as in Figure 4b. It shows the breakdown of O–H bonds and the formation of new bonds. Consequently, ε-FeO_2H experiences a transition process with broken SHBs that leads to dehydration at high temperatures.

After O–H bonds break, it is natural to assume that the H atoms lose the "symmetrization" constraint and become less stable and more volatile at high temperatures. In other words, H atoms are prone to form H_2 molecules. To verify this, we conducted first-principles molecular dynamics (MD) simulation from the TS structure (details in SI). After hundreds of steps (132 fs), the TS structure transits to a combination of ε-

DOI: 10.1021/jacs.7b06528
J. Am. Chem. Soc. 2017, 139, 12129–12132

FeO_2H and Py-phase (see Figure 5S). Meanwhile, H−H pairs form via short-distance diffusion. Our *ab intio* MD simulation results agree with our experimental observation that traces of H were detected from the Raman spectroscopy of the pressure medium.[2]

In summary, our work provides a mechanism of dehydrogenation for high-pressure hydroxyls that feature thermally stable SHB networks. The release of H is driven by a first-order phase transition between two SHB-based structures. Following the most energetically favored transition pathway, half of the SHBs remain essentially intact, but the other half break, causing increased mobility of trapped hydrogen. As a result, ∼50% of H is released during the phase transition. This mechanism has important implications for the chemistry occurring in the Earth's deep interior. Among the previously predicted hydrous minerals that transport water to the deeper part of Earth's mantle,[6,7] the iron-rich Py-phase has a higher density and is gravitationally stable at lower mantle conditions. In Earth's hydrogen cycling, minerals containing FeO_2H could concentrate on the oceanic crust, descend to the mantle through subduction, and finally stabilize in the Py-FeO_2Hx phase by releasing H in the deep mantle. Our work suggests a general mechanism for hydrogen loss in putative FeO_2H-rich patches. Although H_2 molecules are difficult to detect from Earth's surface due to their high mobility, accumulated Py-phase is amenable to investigations involving seismic anomalies. Future investigations, including measuring the seismic, magnetic and electronic properties of Py-FeO_2Hx at conditions mimicking the lower mantle, will provide more information concerning the dehydrogenation process.

■ ASSOCIATED CONTENT

Supporting Information

The Supporting Information is available free of charge on the ACS Publications website at DOI: 10.1021/jacs.7b06528.

Details of experiment and transition pathways reported (PDF)

■ AUTHOR INFORMATION

Corresponding Author

*qingyang.hu@hpstar.ac.cn

ORCID

Qingyang Hu: 0000-0002-2742-3017

Notes

The authors declare no competing financial interest.

■ ACKNOWLEDGMENTS

We thank Z. P. Liu for providing the SSW package. We acknowledge Y. Meng, J. Smith and L. X. Yang for beamline support and A. Gleason for discussion. XRD at the High Pressure Collaborative Access Team (16-IDB) APS, ANL is supported by the DOE-NNSA under award number DE-NA0001974 and by the DOE-BES under award number DE-FG02-99ER45775, with partial instrumentation funding by NSF. S.-C. Zhu is supported by NSFC (Grant No: 21703004). W. L. Mao and Q. Hu acknowledge support from the NSF (EAR-1446969). H.-K. Mao is supported by the NSF (EAR-1345112, EAR-1447438). HPSTAR is supported by NSAF (Grant No: U1530402).

■ REFERENCES

(1) Shieh, S. R.; Mao, H. K.; Hemley, R. J.; Ming, L. C. *Earth Planet. Sci. Lett.* **1998**, *159*, 13.
(2) Hu, Q.; Kim, D. Y.; Yang, W.; Yang, L.; Meng, Y.; Zhang, L.; Mao, H. K. *Nature* **2016**, *534*, 241.
(3) Ohtani, E. *Chem. Geol.* **2015**, *418*, 6.
(4) Evans, B. W. *Int. Geol. Rev.* **2004**, *46*, 479.
(5) Maruyama, S.; Okamoto, K. *Gondwana Res.* **2007**, *11*, 148.
(6) Sano, A.; Ohtani, E.; Kondo, T.; Hirao, N.; Sakai, T.; Sata, N.; Ohishi, Y.; Kikegawa, T. *Geophys. Res. Lett.* **2008**, *35*, 3303.
(7) Tsuchiya, J. *Geophys. Res. Lett.* **2013**, *40*, 4570.
(8) Xu, W.; Greenberg, E.; Rozenberg, G.; Pasternak, M. P.; Bykova, E.; Boffaballaran, T.; Dubrovinsky, L.; Prakapenka, V.; Hanfland, M.; Vekilova, O. Y.; et al. *Phys. Rev. Lett.* **2013**, *111*, 175501.
(9) Ji, M.; Umemoto, K.; Wang, C. Z.; Ho, K. M.; Wentzcovitch, R. M. *Phys. Rev. B: Condens. Matter Mater. Phys.* **2011**, *84*, 1894.
(10) Hermann, A.; Ashcroft, N. W.; Hoffmann, R. *Proc. Natl. Acad. Sci. U. S. A.* **2012**, *109*, 745.
(11) Tsuchiya, J.; Tsuchiya, T. *Phys. Rev. B: Condens. Matter Mater. Phys.* **2011**, *83*, 210.
(12) Gleason, A. E.; Quiroga, C. E.; Suzuki, A.; Pentcheva, R.; Mao, W. L. *Earth Planet. Sci. Lett.* **2013**, *379*, 49.
(13) Hu, Q.; Kim, D. Y.; Liu, J.; Meng, Y.; Yang, L.; Zhang, D.; Mao, W. L.; Mao, H. K. *Proc. Natl. Acad. Sci. U. S. A.* **2017**, *114*, 1498.
(14) Tsuchiya, J.; Tsuchiya, T.; Tsuneyuki, S.; Yamanaka, T. *Geophys. Res. Lett.* **2002**, *29*, 15-1.
(15) Shang, C.; Liu, Z. P. *J. Chem. Theory Comput.* **2013**, *9*, 1838.
(16) Shang, C.; Zhang, X. J.; Liu, Z. P. *Phys. Chem. Chem. Phys.* **2014**, *16*, 17845.
(17) Zhang, X. J.; Liu, Z. P. *J. Chem. Theory Comput.* **2015**, *11*, 4885.
(18) Sheppard, D.; Xiao, P.; Chemelewski, W.; Johnson, D. D.; Henkelman, G. *J. Chem. Phys.* **2012**, *136*, 074103.
(19) Zhu, S. C.; Xie, S. H.; Liu, Z. P. *J. Phys. Chem. Lett.* **2014**, *5*, 3162.
(20) Guan, S. H.; Zhang, X. J.; Liu, Z. P. *J. Am. Chem. Soc.* **2015**, *137*, 8010.
(21) Li, Y. F.; Zhu, S. C.; Liu, Z. P. *J. Am. Chem. Soc.* **2016**, *138*, 5371.
(22) Zhu, S. C.; Xie, S. H.; Liu, Z. P. *J. Am. Chem. Soc.* **2015**, *137*, 11532.
(23) Zhang, X. J.; Liu, Z. P. *Phys. Chem. Chem. Phys.* **2015**, *17*, 2757.
(24) Gleason, A. E.; Jeanloz, R.; Kunz, M. *Am. Mineral.* **2008**, *93*, 1882.
(25) Kresse, G.; Furthmuller, J. *Phys. Rev. B: Condens. Matter Mater. Phys.* **1996**, *54*, 11169.
(26) Blochl, P. E. *Phys. Rev. B: Condens. Matter Mater. Phys.* **1994**, *50*, 17953.
(27) Perdew, J. P.; Burke, K.; Ernzerhof, M. *Phys. Rev. Lett.* **1996**, *77*, 3865.
(28) Zhao, W. N.; Zhu, S. C.; Li, F.; Liu, Z. P. *Chem. Sci.* **2015**, *6*, 3483.
(29) Hu, Q.; Shu, J. F.; Yang, W. G.; Park, C.; Chen, M. W.; Fujita, T.; Mao, H. K.; Sheng, H. W. *Phys. Rev. B: Condens. Matter Mater. Phys.* **2017**, *95*, 104112.
(30) Cai, Y.; Zhang, C.; Feng, Y. P. *Phys. Rev. B: Condens. Matter Mater. Phys.* **2011**, *84*, 094107.
(31) Lü, X.; Yang, W.; Quan, Z.; Lin, T.; Bai, L.; Wang, L.; Huang, F.; Zhao, Y. *J. Am. Chem. Soc.* **2014**, *136*, 419.

DOI: 10.1021/jacs.7b06528
J. Am. Chem. Soc. 2017, 139, 12129−12132